Size Control of Metal Nanoparticle Catalysts for the Gas-Phase Synthesis of Single-Walled Carbon Nanotubes

Takeshi Saito,*,† Satoshi Ohshima,† Wei-Chun Xu,‡ Hiroki Ago,†,§ Motoo Yumura,† and Sumio Iijima†

Research Center for Advanced Carbon Materials, National Institute of Advanced Industrial Science and Technology, Tsukuba 305-8565, Japan, Kashiwa Laboratory, Institute of Research and Innovation, Kashiwa 277-0861, Japan, and Institute for Materials Chemistry and Engineering, Kyushu University, Kasuga 816-8580, Japan

Received: December 21, 2004; In Final Form: March 29, 2005

Nanoparticle catalysts are essential and indispensable for all syntheses of single-walled carbon nanotubes (SWCNTs). We have prepared size-controlled Co, Co−Mo, and Fe−Mo nanoparticles by the reversed micelle method as the catalysts for the gas-phase pyrolytic synthesis of SWCNTs. From the investigation of the relation between the sizes of the nanoparticles and the alkyl-chain lengths of the cationic surfactants, dialkyldimethylammonium bromides, it has been found that the alkyl groups of the surfactants could play a role in controlling the sizes of the nanoparticles and that the alkyl chain of the surfactant should be preferably less than 10 carbon atoms at most to prepare smaller-size nanoparticles with a narrow size distribution. The reduction of the particle size increases the number of nanoparticles in the colloidal solution and leads to a higher yield of SWCNTs.

1. Introduction

Since the discovery of carbon nanotubes (CNTs) in 1991,[1] much attention has been paid to both fundamental and applied research on this promising material. In particular, recent progress in research on the utilization of single-walled carbon nanotubes (SWCNTs), such as for nanoelectronic devices,[2,3] for the tips of scanning probe microscopes,[4] for super-tough fibers,[5,6] for actuators,[7] and so on, has been outstanding, because of their unique structural, mechanical, and electronic properties.

There are many methods used to produce SWCNTs, but they mainly fall into one of the following categories: arc discharge in the presence of metal, laser vaporization of a metal−graphite composite target, carbon monoxide disproportionation on a metal catalyst, and hydrocarbon pyrolysis, generally using a metal catalyst. In all of these categorized methods, the metal nanoparticle is essential and indispensable as the catalyst for the growth of SWCNTs. The size and chemical composition of the metal nanoparticle catalysts determine the diameter and the structural perfection, i.e., the degree of graphitization of the nanotubes.[8]

Recently, we have reported a novel method for synthesizing SWCNTs by the gas-phase hydrocarbon pyrolysis in which the colloidal organic solution of metal nanoparticles prepared by the reversed micelle method is injected directly into a vertical flow reactor,[9] and here we designate this method the direct injection pyrolytic synthesis (DIPS) method. For the controlled synthesis of SWCNTs, it is very important to prepare homogeneous nanoparticles, and the reversed micelle method is known to produce nanoparticles with relatively fine and homogeneous diameters. In the reversed micelle method, a metal chloride is dissolved in a discrete nanoscale water pool surrounded by the self-assembled surfactants, and they act as the reaction cages when the chemical reduction of the metal chloride is carried out. The surfactants stabilize the metal nanoparticles against aggregating with each other and increase the solubility of the nanoparticles in the organic solvent. It should be noted that higher concentrations of metal catalysts are favorable for SWCNT growth in the present method,[9] compared with the other chemical vapor deposition (CVD) growth using the catalyst supported on a substrate or embedded in porous material. Thus, the surfactants are indispensable in the DIPS method for increasing the solubility of the nanoparticles.

We have also reported that the concentration of the thiophene additives to the colloidal solution promotes the CVD reaction,[9] similar to using benzene and ferrocene.[10,11] However, in general, the carbon yield of the CVD growth of SWCNTs is quite low, and that of our CVD reaction was less than 0.1%.[9] Therefore, more improvement of the nanoparticle catalyst, such as reducing the diameter, was needed to increase the yield of SWCNTs. If the nanoparticle catalysts have smaller diameters, then the effective surface area and the catalytic activity should be increased. In this work, we have studied the size control of metal nanoparticles by the reversed micelle method for the effective synthesis of SWCNTs by the DIPS method. We have employed three kinds of dialkyldimethylammonium bromides ($((CH_3)_2(CH_3(CH_2)_n)_2NBr$) with different alkyl-chain lengths ($n = 7$, 9, and 11) as the cationic surfactants to clarify the relation between the alkyl-chain lengths of the surfactants and the sizes of the nanoparticles. The catalytic ability of the nanoparticle catalyst and the quality of the products are also discussed.

* Author to whom correspondence should be addressed. Phone: +81-29-861-4863. Fax: +81-29-861-3392. E-mail: takeshi-saito@aist.go.jp.
† National Institute of Advanced Industrial Science and Technology.
‡ Institute of Research and Innovation.
§ Kyushu University.

10.1021/jp044200z CCC: $30.25
Published on Web 04/29/2005

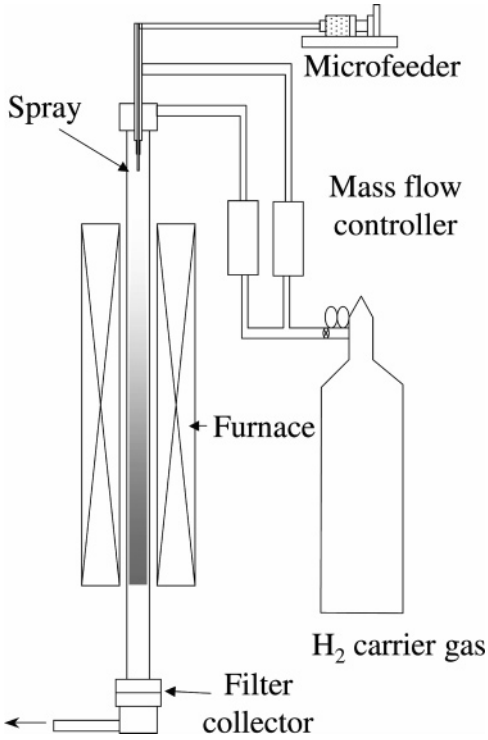

Figure 1. Setup of the direct injection pyrolytic synthesis (DIPS) method. The colloidal solution in the syringe was fed by the microfeeder. SWCNTs are collected at the bottom of the reactor.

2. Experimental Section

The colloidal solutions of the metal nanoparticles were prepared by a reversed micelle method using a procedure based on a previous report.[9] The typical procedure is as follows. Approximately 2.5 mmol of $(CH_3)_2(CH_3(CH_2)_n)_2NBr$ ($n = 7$, 9, or 11), i.e., dimethyldioctylammonium bromide (TCI), didecyldimethylammonium bromide (TCI), or dilauryldimethylammonium bromide (TCI), was dissolved in 10 g of toluene (Wako, GR). In this solution, 0.05 mmol of anhydrous metal chloride was dissolved to make the solution homogeneous. Because these reagents are extremely hygroscopic, all of the above procedures were performed in a glovebox filled with nitrogen gas. Under vigorous stirring, 10 M of $NaBH_4$ aqueous solution was added to the toluene solution (with a concentration of $[BH_4^-]/[Co^{2+}] = 3:1$). Immediately, foaming was caused by the generated hydrogen gas, and the solution turned from light blue to black, suggesting the formation of a colloidal dispersion of metal nanoparticles. After the continuous stirring until it stopped foaming, the dispersion solution was centrifuged at 2390*g* for 2 min and decanted to remove the precipitate from the supernatant. For the transmission electron microscopy (TEM) observation of the nanoparticles to determine their diameters, the sample was prepared by adding the supernatant directly to the TEM microgrid and dried in a vacuum. Note that the higher concentration of the colloidal solutions for the synthesis of SWCNTs was achieved by increasing the concentration of the metal chloride and the surfactants appropriately. Before the CVD reaction, equimolar amounts of thiophene versus the metal atoms were added as a promoter, and this concentrated colloidal solution was employed as a starting material in the DIPS method without any purification procedure. The colloidal solution was stable at room temperature for over 1 month.

The above-mentioned colloidal solution was directly injected into a furnace through a spray nozzle by the hydrogen carrier gas as shown in Figure 1. This solution was fed by a microfeeder at a rate of 65 μL/min under a hydrogen gas flow of 7000 sccm. The inner diameter of the reaction tube was 50 mm, and the length of the furnace was 600 mm. The reaction temperature of the furnace was set at 1200 °C, and the flange at the top of the quartz tube was cooled with water to below 100 °C where the spray nozzle is attached. The mist of the colloidal solution vaporizes simultaneously with the injection, and a reaction occurs to form the carbon product, where toluene vapor and metal nanoparticles act as a carbon source and a catalyst, respectively. In this condition, the residence time of the reactant gas in the furnace was ca. 2.1 s. The reaction product flowed out of the hot zone of the furnace with the carrier gas stream and was collected at the bottom of the quartz tube to achieve semicontinuous growth of SWCNTs.

The diameters of the metal nanoparticles were determined by TEM (JEOL, JEM1010). As-grown carbon nanotubes were observed by scanning electron microscopy (SEM) (Hitachi, S-5000) and TEM and analyzed by resonant Raman scattering (JASCO, NRS-2100) with an Ar ion laser operating at 514.5 nm.

3. Results and Discussion

3.1. Diameter Distribution of Metal Nanoparticles Prepared in the Dilute Micellar Solution. First of all, let us express our cobalt nanoparticles prepared by the reversed micelle method with the three kinds of dialkyldimethylammonium bromides ($(CH_3)_2(CH_3(CH_2)_n)_2NBr$) ($n = 7$, 9, and 11), in terms of Co-7, Co-9, and Co-11, respectively, for simplicity. Similar notations are used for cobalt−molybdenum (CoMo) and iron−molybdenum (FeMo) nanoparticles.

As a beginning, we will examine the cobalt nanoparticles, Co-7, Co-9, and Co-11, prepared normally in the low-concentration reversed micelle solution to avoid aggregation of the nanoparticles. Typical TEM images of Co-7, Co-9, and Co-11 are shown in Figures 2a, 2b, and 2c, respectively. Although the difference in the alkyl-chain length is only 2 or 4 carbon atoms, the sizes of the nanoparticles considerably change depending on the chain length. Namely, we find that the smaller (larger) diameters and narrower (broader) size distributions of the nanoparticles are derived from the reversed micelle system with shorter (longer) alkyl-chain-length surfactants in general. Figures 2d−f are the histograms showing the diameter distributions of the nanoparticles. From a Gaussian fitting of these distributions, the average diameters ± 1 standard deviation of Co-7, Co-9, and Co-11 were estimated to be 2.4 ± 0.8 nm, 4.1 ± 1.6 nm, and 8.7 ± 5.9 nm, respectively. Because of the large diameter and wide distribution of Co-11, the nanoparticle catalyst prepared by using the surfactant with the longest alkyl chains seems to be unsuitable for SWCNT growth. However, the average size of Co-9 is less than half that of Co-11 and slightly larger than that of the typical SWCNT. It was reported that nanoparticles with a diameter of ca. 4 nm could act as the catalyst for the CVD growth of SWCNTs, although the diameters of the synthesized SWCNTs would be relatively large, in agreement with the sizes of the nanoparticles.[12,13]

Most importantly, the average diameter of Co-7 is considerably smaller, and the diameter distribution is extremely narrow. From the average diameters of Co-7 (2.4 nm) and Co-9 (4.1 nm) and the density of the cobalt metal, 8.9 g/cm^3, we can roughly estimate the particle number of a unit weight of Co-7 and Co-9 to be 1.9×10^{18} and 3.9×10^{17} g^{-1}, respectively. Hence, the particle number of a unit weight and, therefore, the actual concentration of the nanoparticles in the colloidal solution of Co-7 are ca. 5 times larger than those of Co-9.

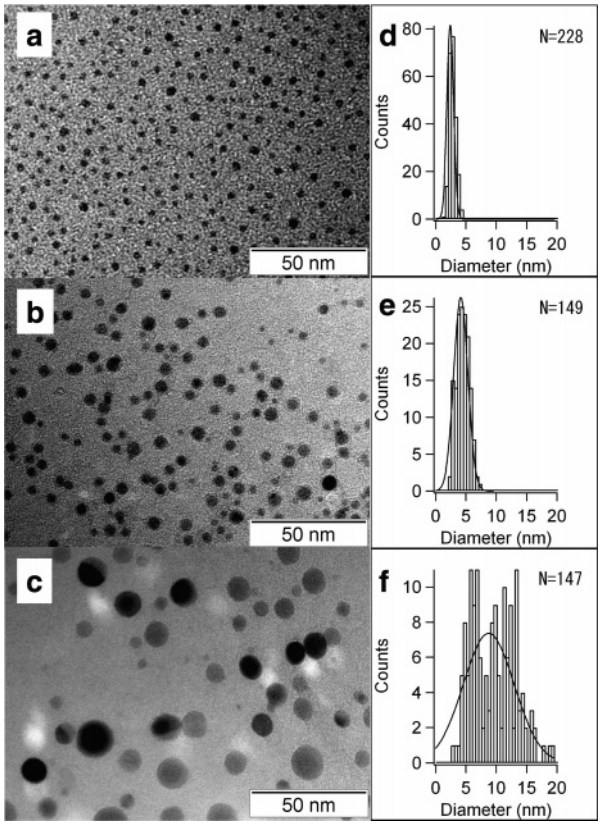

Figure 2. Typical TEM images of the cobalt nanoparticles (a) Co-7, (b) Co-9, and (c) Co-11 produced by the reversed micelle method. Corresponding histograms of the diameter distributions are plotted in parts d, e, and f, respectively. The solid lines correspond to Gaussian fits.

As mentioned above, Co-7 has a considerably smaller diameter and narrower size distribution without any size-separation process, and it is clear that there is a strong relationship between the alkyl-chain length of the surfactant and the size of the nanoparticle. This dependence of the nanoparticle size on the alkyl-chain length could be related to the ability of the self-assembly of these cationic surfactants, because there is no difference in the preparation procedures other than the alkyl-chain length. The reversed micelle is formed by the simplest self-assembly of surfactants, and the surfactants consist of only two moieties, i.e., the nonpolar tails and the polar headgroup. Thus, even the slightest difference in the alkyl chain would considerably increase the stability of the cage structure, and the stable cage of the surfactants should prevent the nanoparticles from aggregating with one another in the chemical reduction process. Hence, homogeneous small nanoparticles with a narrow size distribution would be generated in the stable cage of the surfactants with the small alkyl-chain length. From this point of view, to prepare smaller-size nanoparticles with a narrow size distribution by the reversed micelle method, it would be expected that the surfactant with the relatively small alkyl chain, which is less than 10 carbon atoms, at most, would be selected preferably.

3.2. Diameter Distribution of Metal Nanoparticles Prepared in the Concentrated Micellar Solution. As mentioned above, it is favorable for the effective growth of SWCNTs in the DIPS method to prepare a concentrated colloidal solution of nanoparticles. Moreover, another metal catalyst or a promoter additional metal species should be also considered to improve the ability of the catalyst and accelerate the CVD reaction, such as cobalt−molybdenum (CoMo) and iron−molybdenum (FeMo)

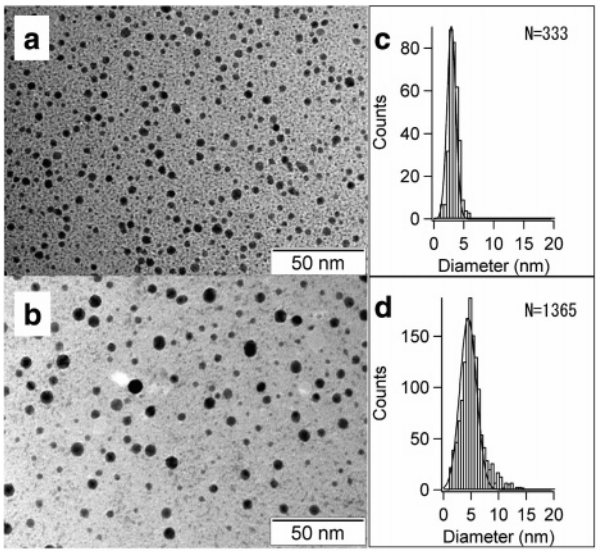

Figure 3. Typical TEM images of (a) CoMo-7 and (b) FeMo-7 produced in the concentrated micelle solutions. Corresponding histograms of the diameter distributions are plotted in parts c and d, respectively. The solid lines correspond to Gaussian fits.

in which the molybdenum metal is employed as a promoter frequently. However, the high concentration of nanoparticles in the reversed micelle solution tends to increase their particle size. Actually, although there are many works targeting the metal nanoparticle prepared by the reversed micelle method,[14] little is known about controlling the sizes of the nanoparticles under the higher-concentration condition. The metal species may also affect the formation process of the nanoparticles and cause the size distribution and the average diameter from the result for Co discussed in the above section to change. Thus, we have investigated the size distribution of CoMo and FeMo nanoparticles prepared in the concentrated reversed micelle system.

The colloidal solutions of the CoMo and FeMo metal nanoparticles, in which the proportion of the molybdenum atom is equal to that of the cobalt or iron metal, were prepared by using the dimethyldioctylammonium bromide ($n = 7$) surfactant with a 25 times higher concentration than that in the above-mentioned Co-7 solution. These nanoparticles are denoted by CoMo-7 and FeMo-7. Note that the catalytic system of CoMo was well-investigated in our previous report[15] and that the optimized proportion of the molybdenum in the CoMo catalyst was Co/Mo = 1:1.

Typical TEM images of the CoMo-7 and FeMo-7 nanoparticles and the diameter distributions measured from these images are shown in Figures 3a−d. The average diameters ±1 standard deviation of the CoMo-7 and FeMo-7 nanoparticles were found to be 2.9 ± 1.0 nm and 4.5 ± 2.1 nm, respectively. The average size and distribution of CoMo-7 are not significantly different from those of Co-7 prepared in the dilute reversed micelle system, but they are slightly larger, most probably due to the aggregation of reversed micelles in the preparation process under the concentrated condition of the micelles. However, the average diameter of the FeMo-7 nanoparticles is larger than that of the CoMo-7 nanoparticles and nearly equal to that of the Co-9 nanoparticles. In general, preparing concentrated solutions of iron nanoparticles is difficult because of their strong ferromagnetic properties, which makes them aggregate with each other, and we speculated that this ferromagnetic interaction would affect the size distribution of FeMo-7 nanoparticles.

3.3. Synthesis of SWCNTs by the DIPS Method. The DIPS method was carried out by using both the CoMo-7 and the

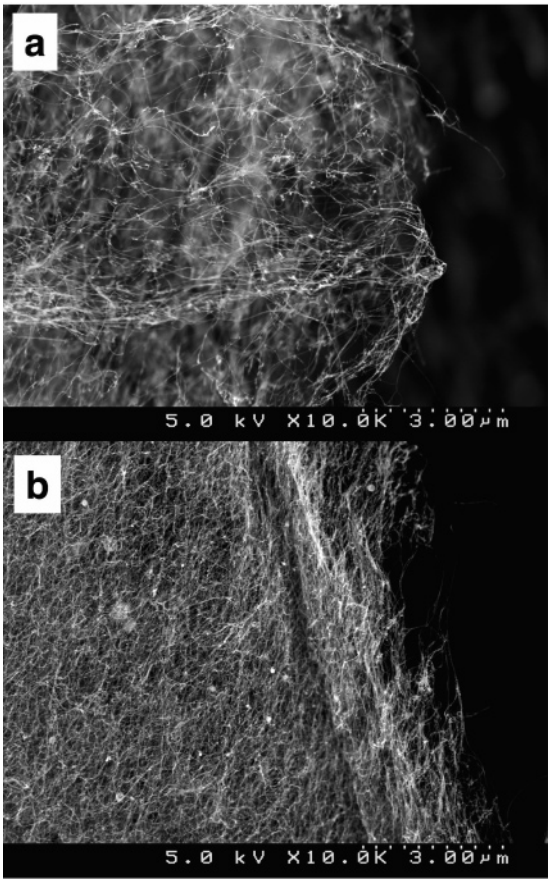

Figure 4. SEM images of the carbon products obtained by the DIPS method using (a) CoMo-7 and (b) FeMo-7 nanoparticle catalysts, respectively. In both products, high densities of entangled carbon nanotube filaments are observed.

FeMo-7 catalysts, and large quantities of weblike and very light carbon materials were obtained in both of the products. Typical SEM images of the carbon products derived from the CoMo-7 and FeMo-7 nanoparticles are shown in Figures 4a and 4b, respectively. These images show a large amount of entangled carbon nanotube filaments, homogeneously distributed over large areas. TEM images of the carbon products of CoMo-7 and FeMo-7 are shown in Figures 5a and 5b, respectively. As shown in Figure 5, almost all of the carbon nanotubes are single-walled in both carbon products of the CoMo-7 and FeMo-7 catalysts. Although we could not obtain accurate histograms of the tube diameters because the observed SWCNTs are highly entangled and bundled with each other, the average diameters evaluated from these TEM images are roughly 2 nm in both products.

To analyze the quality of the carbon products of CoMo-7 and FeMo-7 more closely, we carried out Raman experiments on these products. In Figure 6, Raman scattering spectra in the frequency regions of 1200−1700 and 55−400 cm^{-1} are shown. The strong peak and very weak peak in Figures 6a and 6c are assigned to the tangential mode (G-band) and the disorder-induced mode (D-band), respectively. Concerning the line shape of the G-band peak, a simple analysis can be carried out considering two peaks; one is labeled G^+, for the atomic displacements along the tube axis, and another is G^-, for the modes with atomic displacements along the circumference of the tube. While the frequency of the G^+ mode ($\omega_G{}^+$) is practically independent of the tube diameter, the frequency of the G^- mode ($\omega_G{}^-$) is closely related to the diameter of the SWCNTs, i.e., the curvature of the graphene sheet in the narrow

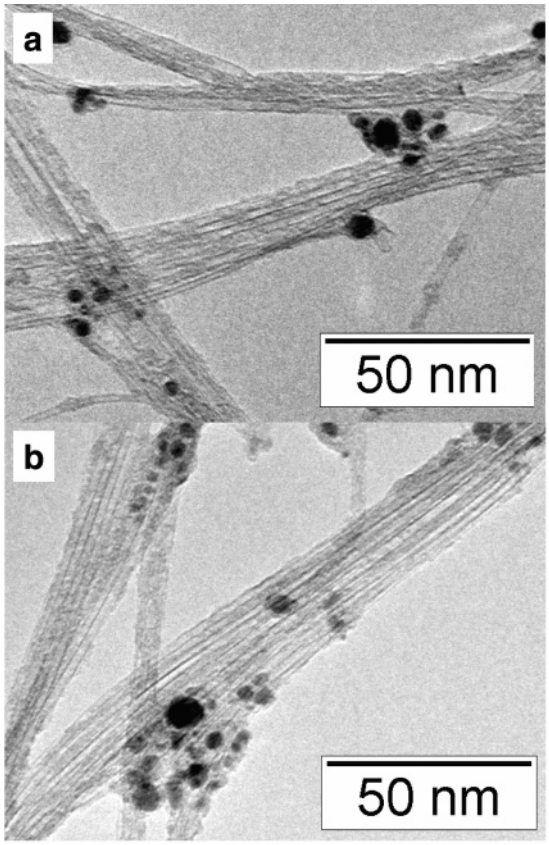

Figure 5. TEM images of the carbon products obtained by using (a) CoMo-7 and (b) FeMo-7 catalysts, showing highly entangled SWCNT bundles.

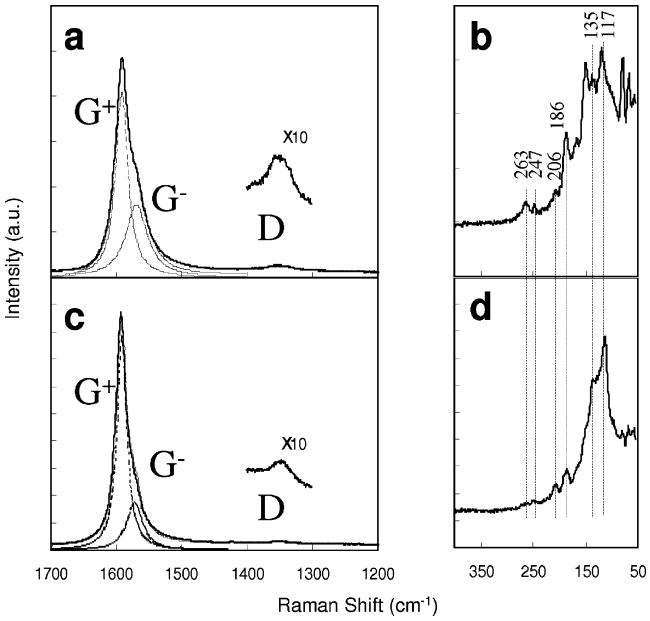

Figure 6. Raman spectra recorded in the ranges 1200−1700 and 100−300 cm^{-1} of the as-grown carbon products obtained by using (a and b) CoMo-7 and (c and d) FeMo-7 catalysts.

SWCNT softens the tangential vibration in the circumferential direction.[16−18] By a Lorentzian line shape analysis, the values of $\omega_G{}^-$ in CoMo-7 and FeMo-7 carbon products are calculated to be 1569 and 1573 cm^{-1}, respectively, and this fact would roughly suggest that the CoMo-7 carbon product is composed of SWCNTs with a slightly narrower diameter distribution than that of FeMo-7. Another remarkable fact is that the D-band peak

is extremely weak and that the line width of the D-band is relatively small (ca. 40 cm^{-1}) compared with those of amorphous carbon in both of the products. These features indicate that there are relatively few defects and amorphous carbon impurities in both of our products.[19,20]

In the low-frequency Raman peaks, a resemblance between the carbon products of CoMo-7 and FeMo-7 was observed as shown in Figures 6b and 6d. These Raman peaks are assigned to radial breathing mode (RBM) vibrations, and the tube diameter d can be estimated by using the relation $d = 248/\omega_{RBM}$,[21] where ω_{RBM} is the RBM vibration frequency observed. The main RBM peak common to both spectra of CoMo-7 and FeMo-7 is at 117 cm^{-1}, and this peak corresponds to a diameter of 2.1 nm by using the above-mentioned relation. This diameter is consistent with the average diameter roughly evaluated from the TEM observation. It should be noted that our Raman results showed that there is a relatively broad peak in the range of 100−200 cm^{-1}, and this range corresponds to the diameter range of ca. 1.2−2.5 nm. The reason that our Raman results seem to be biased toward one size, i.e., 2 nm, might be that our SWCNTs have a relatively broad diameter distribution.

The other common RBM peaks of two carbon products at 135, 186, and 206 cm^{-1} correspond to the diameters of 1.8, 1.3, and 1.2 nm, respectively. Moreover, the RBM peaks of the higher frequencies, 247 and 263 cm^{-1}, are also observed in the CoMo-7 product, which suggests that considerably smaller SWCNTs with a diameter of less than 1 nm could exist, although RBM peaks with such high frequencies have hardly been observed in the FeMo-7 product. As discussed above, the Raman analysis of the carbon products shows that the CoMo-7 catalysts produce SWCNTs with a slightly narrower diameter distribution than that of FeMo-7; however, this result is not completely consistent with the rather large difference in the average diameters between the CoMo-7 and FeMo-7 nanoparticles. This fact would suggest that the diameter distribution of SWCNTs would not be decided by the size distribution of the original catalysts in our method. The most likely explanation for this inconsistency is that only the smaller nanoparticles act as catalysts in our DIPS method. From the TEM results, it is shown that the size distributions of the nanoparticle catalysts have widths of 1.5−5 nm in CoMo-7 and of 1.5−10 nm in FeMo-7, respectively. The reactivity of the nanoparticle catalysts would be different according to their sizes, and smaller nanoparticles would have higher reactivities. Moreover, the reaction time is extremely short in our system compared with the other CVD growth methods using the catalyst supported on a substrate or embedded in a porous material, because the residence time of the nanoparticle catalysts is ca. 2.1 s. Therefore, the above-mentioned explanation that only the highly reactive nanoparticles can act as catalysts in our system should be convincing. However, another explanation could also be thought of as follows. Recently, we have reported that there is a rather large difference in the size distribution of nanoparticle catalysts before and after CVD growth and suggested as the possible explanation that the original nanoparticles (average diameter 10.8 nm) may split into smaller ones (1−5 nm) in the furnace.[15] Similarly, in present work, the size distribution of the catalysts might be changing in the furnace by splitting or shrinking. The extremely high reaction temperature at 1200 °C might be one of the reasons for the changing size distribution of the nanoparticles in the furnace. More detailed dynamic observation of the catalysts in the furnace would be needed to clarify the formation mechanism of SWCNTs in our DIPS method.

Let us now consider the carbon yield of CoMo-7 and FeMo-7 products to evaluate the abilities of these catalysts. Note that the carbon yield means the weight percentage of the as-grown carbon products against the total of the injected carbon atom. The carbon yield of the CoMo-7 product was estimated to be around 0.46%, and this value is ca. 5 times larger than that obtained by using the colloidal solutions of CoMo-9 catalyst as we reported previously.[9] It should be noted that this difference between CoMo-7 and CoMo-9 in the carbon yield value is in very good numerical agreement with the difference in the particle number of a unit weight of Co-7 and Co-9 as described above. On the basis of the similarity in the diameter distribution between Co-7 and CoMo-7, Co-9 and CoMo-9 would be expected to have a similar distribution of particle diameters. Therefore, it can be supposed that the carbon yield in the gas-phase CVD growth of SWCNTs would mainly depend on the number of nanoparticle catalysts. In other words, we can safely assume that the greater the number of nanoparticle catalysts, the greater the carbon yield, if catalytic nanoparticles are composed of the same metal species. To confirm this hypothesis more directly, we employed the half-diluted CoMo-7 colloidal solution as the starting material in the DIPS method. The carbon yield of the product was estimated to be 0.2%, and this value is consistent with this hypothesis about the yield.

However, the carbon yield of the product obtained by using the FeMo-7 catalyst was estimated to be 0.99%. This yield value is over 2 times larger than that produced by using the CoMo-7 catalyst. This fact would suggest that the performance of the iron catalyst for graphitization is superior to that of the cobalt in the DIPS method. Note that even in the HiPco process, which is one of the most famous methods for the large-scale production of SWCNTs, the yield based on the injected carbon monoxide was reported to be less than 0.02%.[22,23] From this point of view, our DIPS method could be a very promising method to produce SWCNTs on a large scale.

4. Conclusions

We have prepared nanoparticle catalysts by the reversed micelle method employing dialkyldimethylammonium bromides as the cationic surfactants and studied the size controllability of the nanoparticle by changing the alkyl-chain length of the surfactants. From the diameter distribution of the nanoparticles obtained by the TEM observations, it has been suggested that the smaller (larger) diameter and narrower (broader) size distributions of the nanoparticles are derived from the reversed micelle system with shorter (longer) alkyl-chain-length surfactants in general. We believe that this controllability of the nanoparticle size is presumably due to the difference in the self-assembly abilities of micelles with various alkyl-chain lengths. SWCNTs are synthesized from the colloidal solution of the CoMo and FeMo nanoparticles prepared by this method, and we have found that the carbon yield in the gas-phase CVD synthesis directly depends on the number of nanoparticles.

Acknowledgment. This work was partially supported by the Nano-Carbon Technology project of the Ministry of Economy, Trade and Industry, Japan. T.S. thanks Ms. Y. Ikeda for experimental assistance.

References and Notes

(1) Iijima, S. *Nature* **1991**, *354*, 56−58.
(2) Collins, P. G.; Arnold, M. S.; Avouris, P. *Science* **2001**, *292*, 706−709.
(3) Lee, J. U.; Gipp, P. P.; Heller, C. M. *Appl. Phys. Lett.* **2004**, *85*, 145−147.

(4) Wong, S. S.; Joselevich, E.; Woolley, A. T.; Cheung, C. L.; Lieber, C. M. *Nature* **1998**, *394*, 52−55.

(5) Vigolo, B.; Pénicaud, A.; Coulon, C.; Sauder, C.; Pailler, R.; Journet, C.; Bernier, P.; Poulin, P. *Science* **2000**, *290*, 1331−1334.

(6) Dalton, A. B.; Collins, S.; Muñoz, E.; Razal, J. M.; Ebron, V. H.; Ferraris, J. P.; Coleman, J. N.; Kim, B. G.; Baughman, R. H. *Nature* **2003**, *423*, 703.

(7) Baughman, R. H.; Cui, C.; Zakhidov, A. A.; Iqbal, Z.; Barisci, J. N.; Spinks, G. M.; Wallace, G. G.; Mazzoldi, A.; Rossi, D. D.; Rinzler, A. G.; Jaschinski, O.; Roth, S.; Kertesz, M. *Science* **1999**, *284*, 1340−1344.

(8) Laurent, C.; Flahout, E.; Peigney, A.; Rousset, A. *New J. Chem.* **1998**, 1229−1237.

(9) Ago, H.; Ohshima, S.; Uchida, K.; Yumura, M. *J. Phys. Chem. B* **2001**, *105*, 10453−10456.

(10) Cheng, H. M.; Li, F.; Su, G.; Pan, H. Y.; He, L. L.; Sun, X.; Dresselhaus, M. S. *Appl. Phys. Lett.* **1998**, *72*, 3282−3284.

(11) Cheng, H. M.; Li, F.; Sun, X.; Brown, S. D. M.; Pimenta, M. A.; Marucci, A.; Dresselhaus, G.; Dresselhaus, M. S. *Chem. Phys. Lett.* **1998**, *289*, 602−610.

(12) Cheung, C. L.; Kurtz, A.; Park, H.; Lieber, C. M. *J. Phys. Chem. B* **2002**, *106*, 2429−2433.

(13) Li, Y.; Kim, W.; Zhang, Y.; Rolandi, M.; Wang, D.; Dai, H. *J. Phys. Chem. B* **2001**, *105*, 11424−11431.

(14) For example, Martino, A.; Stoker, M.; Hicks, M.; Bartholomew, C. H.; Sault, A. G.; Kawola, J. S. *Appl. Catal., A* **1997**, *161*, 235−248 and references therein.

(15) Ago, H.; Ohshima, S.; Tsukagoshi, K.; Tsuji, M.; Yumura, M. *Curr. Appl. Phys.*, in press.

(16) Kasuya, A.; Sasaki, Y.; Saito, Y.; Tohji, K.; Nishina, Y. *Phys. Rev. Lett.* **1997**, *78*, 4434−4437.

(17) Jorio, A.; Filho, A. G. S.; Dresselhaus, G.; Dresselhaus, M. S.; Swan, A. K.; Ünlü, M. S.; Goldberg, B. B.; Pimenta, M. A.; Hafner, J. H.; Lieber, C. M.; Saito, R. *Phys. Rev. B* **2002**, *65*, 1554121−1554129.

(18) Jorio, A.; Pimenta, M. A.; Filho, A. G. S.; Samsonidze, G. G.; Swan, A. K.; Ünlü, M. S.; Goldberg, B. B.; Saito, R.; Dresselhaus, G.; Dresselhaus, M. S. *Phys. Rev. Lett.* **2003**, *90*, 1074031−1074034.

(19) Jorio, A.; Pimenta, M. A.; Filho, A. G. S.; Saito, R.; Dresselhaus, G.; Dresselhaus, M. S. *New J. Phys.* **2003**, *5*, 139.

(20) Jorio, A.; Fantini, C.; Dantas, M. S. S.; Pimenta, M. A.; Filho, A. G. S.; Samsonidze, G. G.; Brar, V. W.; Dresselhaus, G.; Dresselhaus, M. S.; Swan, A. K.; Ünlü, M. S.; Goldberg, B. B.; Saito, R. *Phys. Rev. B* **2002**, *66*, 1154111−1154118.

(21) Jorio, A.; Saito, R.; Hafner, J. H.; Lieber, C. M.; Hunter, M.; McClure, T.; Dresselhaus, G.; Dresselhaus, M. S. *Phys. Rev. Lett.* **2001**, *86*, 1118−1121.

(22) Bronikowski, M. J.; Williams, P. A.; Colbert, D. T.; Smith, K. A.; Smalley, R. E. *J. Vac. Sci. Technol., A* **2001**, *19*, 1800−1805.

(23) Nikolaev, P.; Bronikowski, M. J.; Bradley, K.; Rohmund, F.; Colbert, D. T.; Smith, K. A.; Smalley, R. E. *Chem. Phys. Lett.* **1999**, *313*, 91−97.